Journal of Applied Polymer Science

Effects of Calcium Carbonate and Compounding Sequence on the Phase Morphology and Properties of Maleic Anhydride-Grafted Polypropylene Compatibilized Polyamide 6/Polypropylene Blend

Li Wang, Xue-Liang Ling, Chen Shi, Zhao-Xia Guo, Jian Yu

Key Laboratory of Advanced Materials (MOE), Department of Chemical Engineering, Tsinghua University, Beijing 100084, People's Republic of China

Correspondence to: Z.-X. Guo (E-mail: guozx@mail.tsinghua.edu.cn) or J. Yu (E-mail: yujian03@mail.tsinghua.edu.cn)

ABSTRACT: Effects of calcium carbonate ($CaCO_3$) and compounding sequence on the phase morphology of maleic anhydride-grafted polypropylene (MAPP) compatibilized polyamide 6 (PA6)/polypropylene (PP) blend were investigated. The morphology in the subskin and core regions of injection molded specimen was observed using scanning electron microscopy, which shows great changes due to the incorporation of $CaCO_3$. With the addition of $CaCO_3$ (25 phr), oriented "ginger-like" network (directly mixing) or loose elongated network (mixing PA6, PP, and MAPP with premixed PA6/$CaCO_3$ masterbatch) of PP phase is formed in the core region, instead of spherical dispersed PP domains for unfilled blend. The distribution of $CaCO_3$ in PA6 and PP phases was determined by selectively dissolving PA6 phase and thermogravimetric analysis of PP phase. A possible mechanism is proposed based on the morphology evolution process to interpret the morphological differences. The mechanical properties and heat distortion temperature of the materials were tested and correlated with the morphology formed. © 2012 Wiley Periodicals, Inc. J. Appl. Polym. Sci. 000: 000–000, 2012

KEYWORDS: calcium carbonate; sequence; morphology; distribution; mechanism; property

Received 8 November 2011; accepted 14 February 2012; published online 00 Month 2012
DOI: 10.1002/app.37535

INTRODUCTION

Blending of polymers provide a chance of combining the advantages of different polymers and achieving optimized overall properties. Many polymer blending systems have been investigated thoroughly and some have been commercialized. It is common knowledge that most polymer pairs are thermodynamically immiscible and different types of phase-separated morphology can be formed when they are mixed. The properties of immiscible polymer blends are closely related to the morphology formed during processing.[1] Thus, tailoring the morphology of polymer blends has become an important way in optimizing the properties of polymer blends. Traditionally, a compatibilizer is often used to obtain fine morphology.[2]

Recent studies have revealed the great potential of inorganic fillers in tailoring the morphology of polymer blends. For instance, the incorporation of organoclay (nanofiller) can bring about a significant reduction in the average domain size of polymer blends with matrix-dispersed type morphology[3–5] or a change from sea-island morphology to cocontinuous morphology.[6–8] The influence of traditional microsized fillers (talc, glass fibers, glass beads, microsized calcium carbonate, etc.) on the morphology of polymer blends has also been reported.[9–12]

Microsized calcium carbonate is the second most commonly used filler in industry after talc. Usually, it is incorporated into polyolefin/elastomer systems to obtain balanced stiffness, strength, and toughness.[13–20] Here two extreme situations of phase structure can be formed: (1) $CaCO_3$ and elastomer are dispersed separately in polymer matrix and (2) $CaCO_3$ particles are encapsulated by the elastomer. The location of $CaCO_3$ can be controlled by justifying the interactions between $CaCO_3$ and polymers[19] or changing mixing sequences.[20] According to the results of many researchers,[19,20] different phase structures may affect the reinforcement and toughening of polymer blends significantly. Despite considerable amount of research on $CaCO_3$-filled polymer blends, current studies are insufficient in the following two aspects:

1. Usually, injection molded specimen is cryofractured perpendicular to the injection flow direction and morphology

Table I. Composition and Designations

	PA6	PP	MAPP	$CaCO_3$	Compounding sequence
PA6/PP/5M	70	25	5	0	One-step compounding
PA6/PP/25C	70	30	0	25	One-step compounding
PA6/PP/5M/25C-1	70	25	5	25	One-step compounding
PA6/PP/5M/25C-2	70	25	5	25	Masterbatch approach 1° PA6+$CaCO_3$ (7 : 3) 2° (PA6/$CaCO_3$)+PA6+PP+MAPP

observation is carried out on the core region of fractured surface. This custom is suitable for typical sea-island morphology (spherical dispersed domains). Nevertheless, when the addition of filler alters the sea-island morphology greatly into complicated morphology (e.g., cocontinuous), this custom becomes too simple to obtain a clear and accurate description of the morphology formed.[21]

2. The distribution of filler, which is an important factor in determining the final properties of filled polymer blends, is usually obtained based on microscopic analysis (optic microscopy, scanning, or transmission electron microscopy). The result is not quantitative and thus a deep understanding of structure–property relationship for filled polymer blends is often not possible.

The present work aims at overcoming these obstacles in the investigation of filled polymer blend. PA6/PP blend is selected as a model system because it is a typical immiscible system possessing both research interest and industrial value, due to its mutually complementary properties.[22] Maleic anhydride-grafted polypropylene (MAPP) is used as compatibilizer and $CaCO_3$ is selected as filler. To our knowledge, the effect of $CaCO_3$ on the morphology of PA6/PP blend has rarely been reported in literature.[23] In the present work, the effects of $CaCO_3$ and compounding sequence on the morphology of PA6/PP/MAPP (70/25/5) blend have been investigated thoroughly and interpreted. The distribution of $CaCO_3$ in PA6 and PP phases has been determined quantitatively. The mechanical properties and heat distortion temperature (HDT) of both unfilled and $CaCO_3$-filled PA6/PP/MAPP blends have been tested and correlated with the morphology formed.

EXPERIMENTAL

Materials

PA6 (B3S, MFI: 29.4 g/10 min) was purchased from BASF (Malaysia). PP (S1003, MFI: 3.2 g/10 min) was obtained commercially from Yanshan Petroleum and Chemical (Beijing, China). MAPP with 1 wt % of MA was prepared by reactive extrusion in our laboratory. $CaCO_3$ (WF1250, mesh: 1250) was supplied by Guoli Super Fine Powder Co., Ltd. (Beijing, China).

Preparation of unfilled and $CaCO_3$-filled PA6/PP Blends

PA6 and $CaCO_3$ were dried at 110°C for 4 h prior to compounding. All materials were premixed manually and then extruded using a counter-rotating twin-screw extruder [TE-34, KY Chemical Machinery (Nanjing, China)]. The mixing temperature was 200, 230, 230, 235, and 225°C from hopper to die and the screw speed was 120 r min^{-1}. After being granulated and dried, the extrudates were injection molded using an injection molder [ZT-630, Zhenda Machinery (Hangzhou, China)] into standard specimens for tensile and impact tests. The injection temperature was 230°C and the mould was kept at ambient temperature. The composition and designations of all samples are given in Table I.

Characterization

Field Emission Scanning Electron Microscopy (FESEM). Morphology observation was conducted with a JEOL JSM-7401F apparatus operating at an accelerating voltage of 1 kV. The samples were prepared in three ways: (1) cryofractured in liquid nitrogen; (2) remove PA6 phase by solvent dissolution using hexafluroisopropanol (HFIP) repeatedly and get PP phase; (3) remove PP phase by Soxhlet extraction using xylene as solvent. A JEOL software (SMILEVIEW) was used to measure the mean size of PP phase.

Thermogravimetric Analysis (TGA). TGA (TA Instruments TGA2050) was performed on the PP phase after removing PA6 phase by solvent dissolution to determine the amount of $CaCO_3$ in PP phase. The conditions are: heating from ambient temperature to 600°C at a heating rate of 20°C min^{-1}; N_2 atmosphere.

Mechanical Test. The tensile and flexural properties of all samples were tested using a TCS-2000 tensile tester (Gotech). The tensile test was conducted according to GB1040-1979 at a testing rate of 50 mm min^{-1} and the flexural test was conducted according to GB1042-1979 at a testing rate of 10 mm min^{-1}. The notched Izod impact strength of all samples was tested according to GB1843-1980 using a UJ-40 impact testing machine (Hebei Testing Machinery (Chengde, China), energy pendulum: 2 J). Before dry state mechanical test, all specimens were dried in a vacuum oven for 6 h. Before wet state mechanical test, all specimens were kept at 25°C and under relative humidity of 50% for 48 h.

Heat Distortion Temperature (HDT). The HDT of all samples were tested using a HV-2000 HDT tester (Gotech) according to GB1634-2000.

RESULTS AND DISCUSSION

Morphology

To obtain a clear reveal of the morphology of all samples, the injection molded tensile specimens were cryofractured both perpendicular and parallel to the flow direction for morphology observation, as is shown in Figure 1. Besides, PP phase which

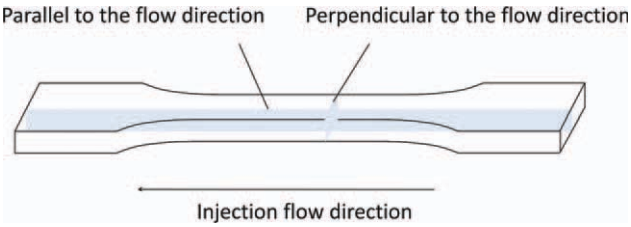

Figure 1. Fractured surfaces along two directions for morphology observation. [Color figure can be viewed in the online issue, which is available at wileyonlinelibrary.com.]

was recovered by dissolving PA6 phase using HFIP was also characterized by FESEM.

Figure 2 shows the FESEM images of sample PA6/PP/5M. It has been reported that during the process of injection molding, a hierarchical structure of morphology called skin-core structure [including skin, subskin (or shear zone), and core] is often formed.[24–27] The skin layer is quite a thin layer which is formed when molten material enters mould, undergoes stretching to some extent and solidifies quickly. Thus, in the present study we will only concern about the subskin and core regions below skin layer.

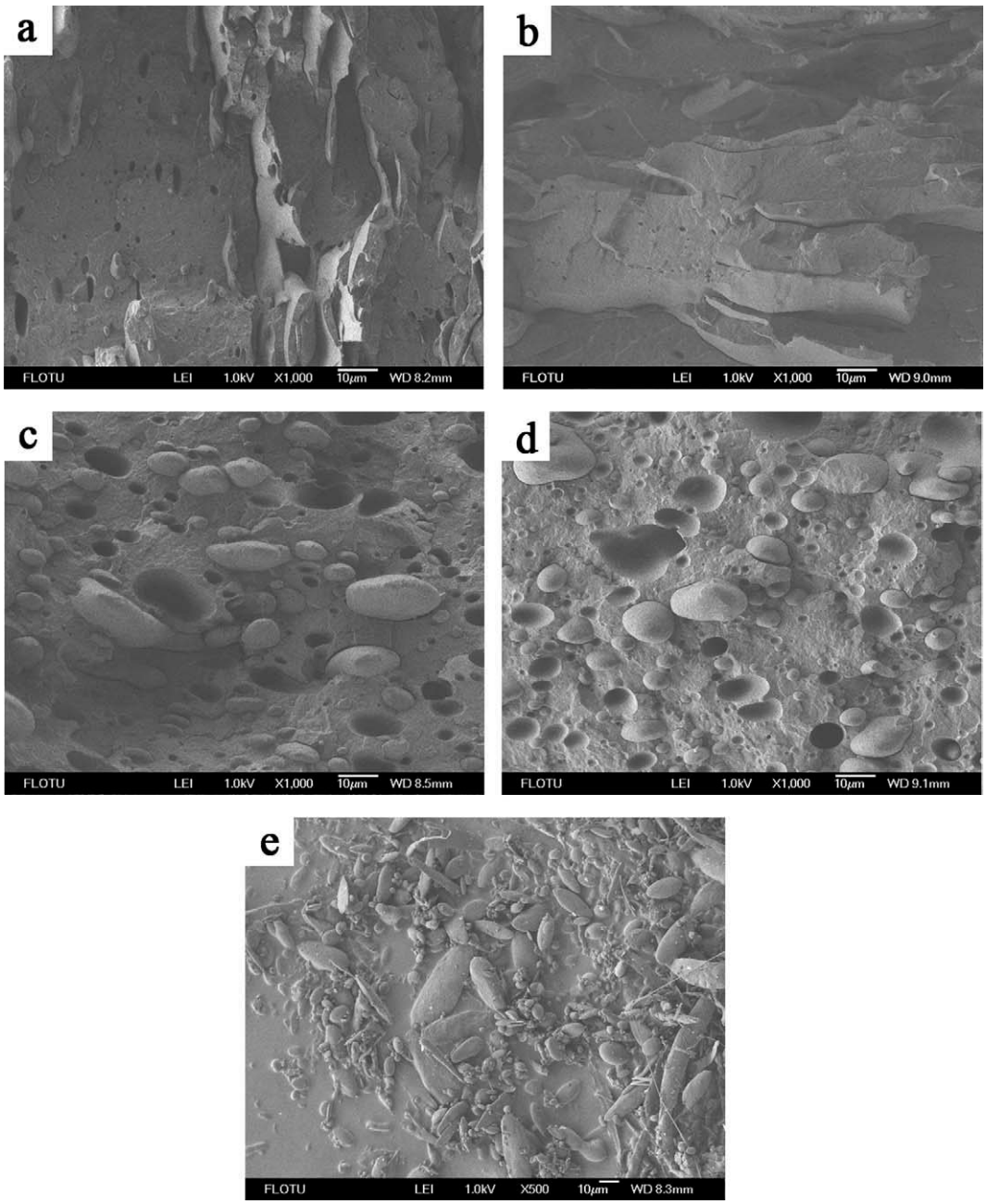

Figure 2. FESEM images of sample PA6/PP/5M: (a) perpendicular to flow direction, subskin; (b) parallel to flow direction, subskin; (c) perpendicular to flow direction, core; (d) parallel to flow direction, core; (e) recovered PP phase.

Applied Polymer SCIENCE

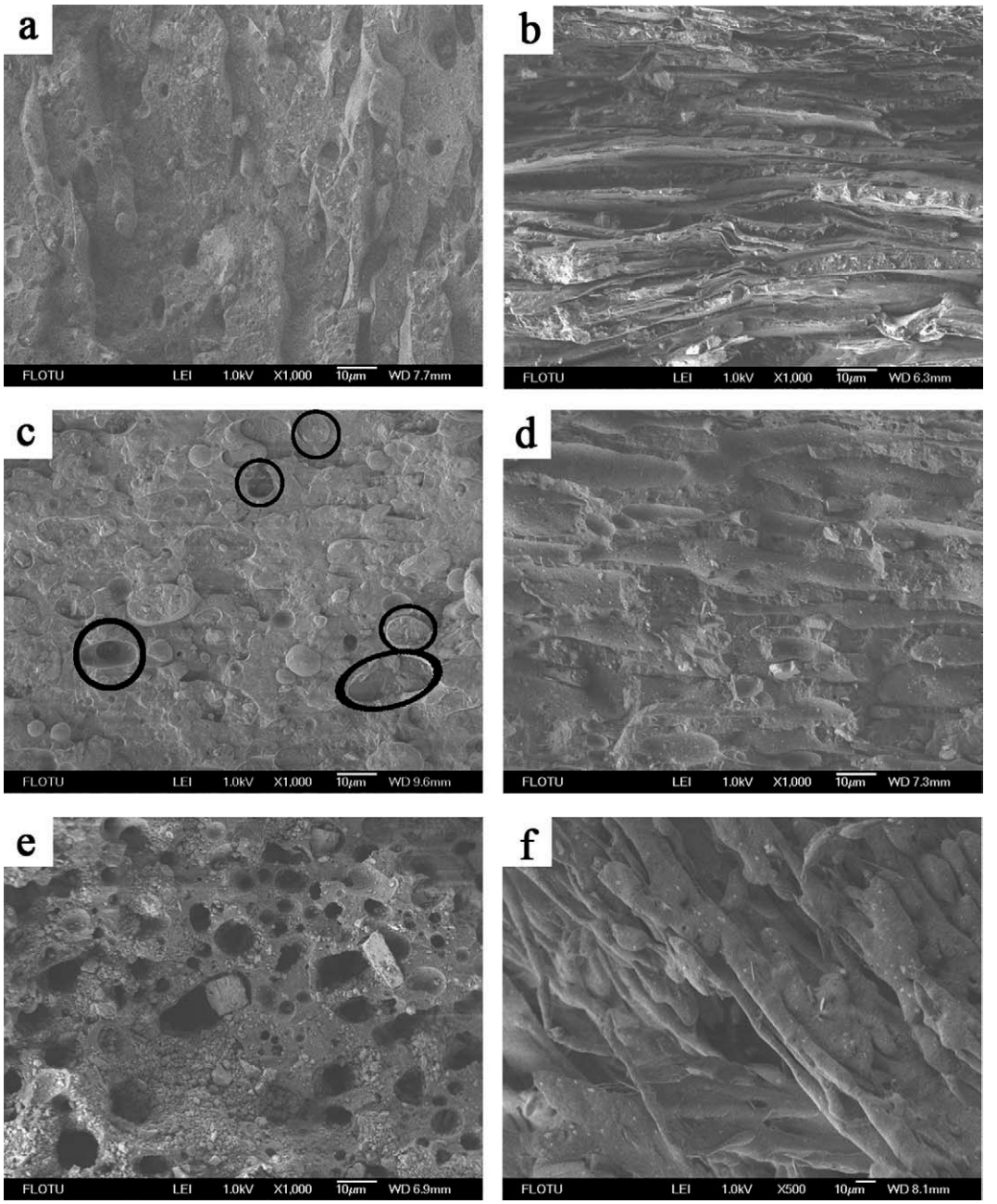

Figure 3. FESEM images of sample PA6/PP/5M/25C-1: (a) perpendicular to flow direction, subskin; (b) parallel to flow direction, subskin; (c) perpendicular to flow direction, core; (d) parallel to flow direction, core; (e) perpendicular to flow direction, with PP etched by xylene extraction, core; (f) recovered PP phase.

For sample PA6/PP/5M, platelets parallel to each other can be observed from fractured surfaces perpendicular and parallel to the melt flow direction in the subskin region, with their thickness ranging from 2 to 10 μm. In the direction perpendicular to the melt flow direction [Figure 2(a)], some platelets can reach 50 μm in length, while some others are only several μm in length. In the direction parallel to the melt flow direction [Figure 2(b)], the length of the platelets is larger.

In the core region, from both fracture surfaces [Figure 2(c,d)] only semispherical and semiellipsoidal bulges can be found, indicating PP phase is dispersed as spherical or ellipsoidal domains in the core region. The mean size of dispersed domains was measured to be 6.2 μm, which is quite large. The interfaces between PA6 and PP phase are sharp and holes left after dispersed particles falling out from matrix phase can be clearly seen. The large dispersed domain size and poor interfacial adhesion indicate that the compatibility between PA6 and PP is not good enough even in the presence of MAPP.

Figure 2(e) is the FESEM image of the dispersed phase of PA6/PP/5M, which was obtained by removing the continuous PA6

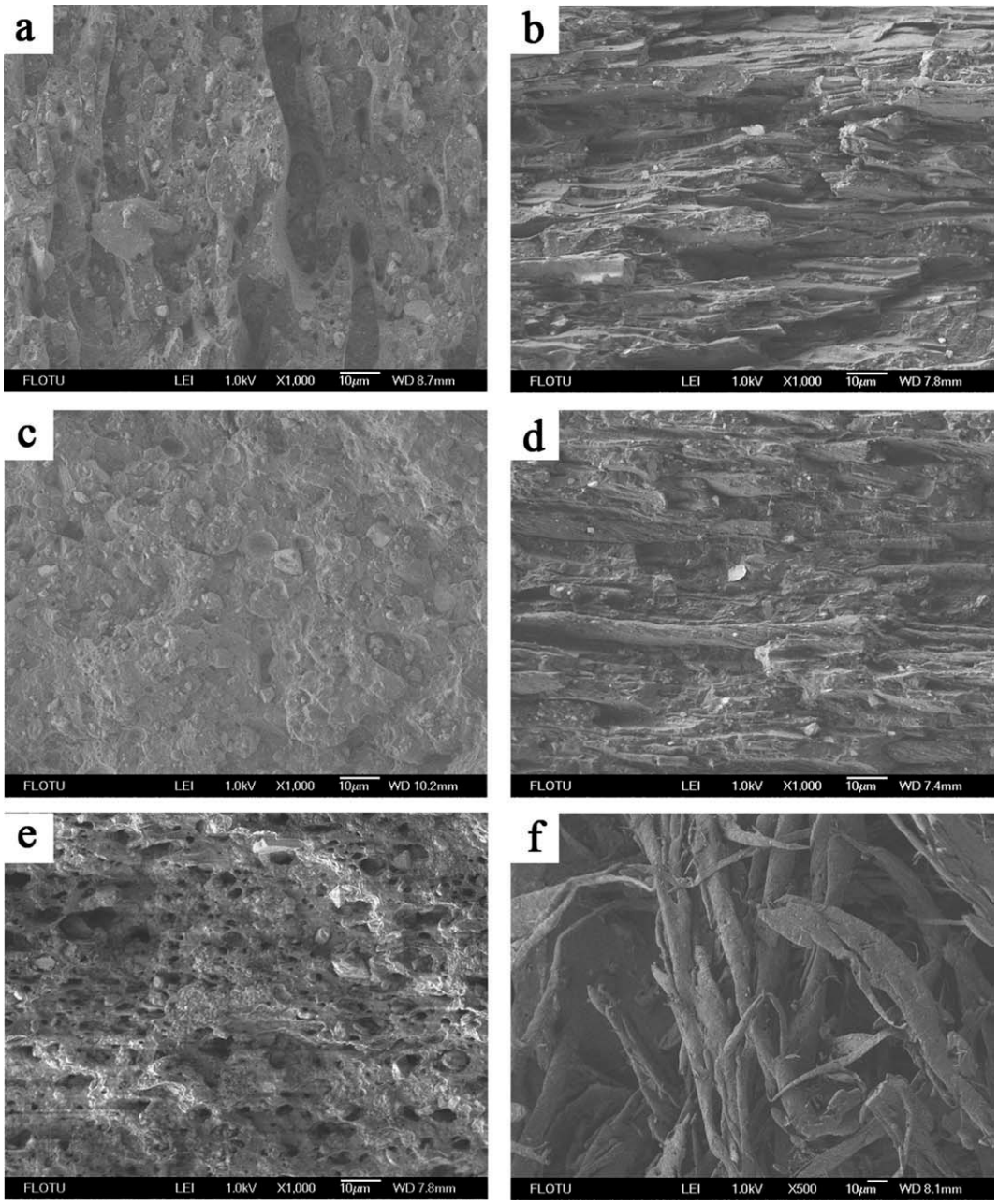

Figure 4. FESEM images of sample PA6/PP/5M/25C-2: (a) perpendicular to flow direction, subskin; (b) parallel to flow direction, subskin; (c) perpendicular to flow direction, core; (d) parallel to flow direction, core; (e) perpendicular to flow direction, with PP etched by xylene extraction, core; (f) recovered PP phase.

phase using HFIP. Fibrils, rods, ellipsoids, and spheres can be clearly seen.

Figure 3 shows the results of morphology observation on sample PA6/PP/5M/25C-1. From Figure 3(a,b) it can be found that irregular shape platelets coexist with fibrils and strips. The thickness of these domains is smaller than 10 μm and their length along the melt flow direction can reach 50 μm. In the core region, not only semispherical bulges but some round or elliptical fractured surfaces [circled out in Figure 3(c)] also show up on the fractured surface perpendicular to the flow direction, which is apparently different from that for PA6/PP/5M. A combination of Figure 3(c,d) reveals that these fracture PP domains exist as strips that are oriented along the flow direction and lumps or nodes are present on these strips. It is quite interesting to see from Figure 3(f) that the strips don't exist separately but conglutinate to each other through the nodes, forming oriented network or so-called "ginger-like" structure. Therefore, PP phase in the core region presents coexistence of spherical domains and oriented ginger-like structure. The average diameters of spherical dispersed domains and the strips are 4.2 and 7.1 μm, respectively.

The distribution of $CaCO_3$ in the two phases can be determined qualitatively from Figure 3(e). After Soxhlet extraction using

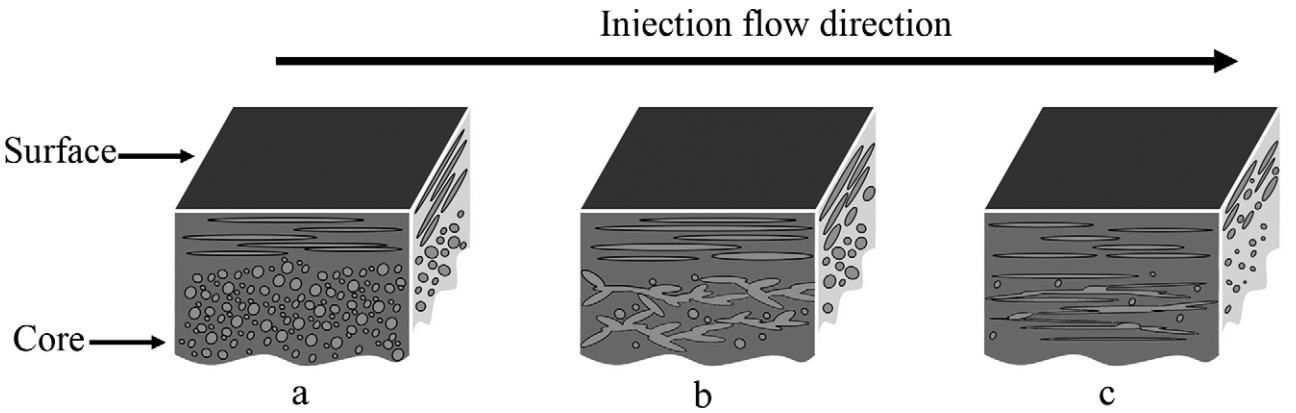

Figure 5. Sketch illustrating the distribution of morphology in each injection-molded sample (left: PA6/PP/5M; middle: PA6/PP/5M/25C-1; right: PA6/PP/5M/25C-2).

xylene, PP phase was removed, leaving many holes on the fractured surface. A lot of $CaCO_3$ can be observed in and around of the holes, which is a clear sign that a large amount of $CaCO_3$ is distributed in PP phase. This will be verified by TGA in following analysis.

Figure 4 shows the FESEM images of sample PA6/PP/5M/25C-2, which was prepared by the masterbatch approach (premixed PA6/$CaCO_3$ masterbatch was mixed with desired amounts of PA6, PP and MAPP). In the subskin region, PP phase still exist as platelets, fibrils and strips. In the core region, it can be found that the phase morphology changes significantly. First, the phase morphology becomes finer, considering that the spherical dispersed particles has a mean diameter of 2.2 μm and the average diameter of the strips is 3.2 μm, which are all well below those of PA6/PP/5M/25C-1. Second, nodes also exist in the strips of PA6/PP/5M/25C-2, but their density is much lower than that of PA6/PP/5M/25C-1. This means that in the core region of PA6/PP/5M/25C-2, finer and looser elongated network structure of PP phase is formed.

In Figure 4(e) a lot of $CaCO_3$ particles can also be observed in the holes left by the removal of PP phase, indicating that a certain amount of $CaCO_3$ is present in PP phase finally, although $CaCO_3$ was mixed with PA6 first.

Figure 5 presents a schematic illustration of the skin-core morphology in each injection-molded sample (PA6/PP/5M, PA6/PP/5M/25C-1, and PA6/PP/5M/25C-2).

Distribution of $CaCO_3$ in the Two Phases

The addition of $CaCO_3$ induces significant changes in the phase morphology of PA6/PP/MAPP (70/25/5) blend and great differences in morphology are found between $CaCO_3$-filled blend prepared by different compounding sequences. It is well known that the morphology of polymer blends mainly depends on blending composition, viscosity ratio, interfacial tension, processing parameters and so on. The distribution of $CaCO_3$ in PA6 and PP phases is an important factor for morphology evolution, because different distribution states of $CaCO_3$ can cause variation in viscosity ratio between PP and PA6 phase. To determine the distribution states of $CaCO_3$, TGA was carried out on the recovered PP phase after the removal of PA6 phase using HFIP. The content of $CaCO_3$ in PP phase can be determined according to the weight percentage of residue in TGA. By further estimation, the distribution ratio of $CaCO_3$ in PP and PA6 phases can be obtained and the results are shown in Table II.

For PA6/PP/5M/25C-1, which was prepared by compounding all components simultaneously, 74.6 % of the incorporated $CaCO_3$ is distributed in PP phase finally. For PA6/PP/5M/25C-2, the amount of $CaCO_3$ in PP phase is 53.3%, which is smaller than that for PA6/PP/5M/25C-1. The discrepancy in the distribution states of $CaCO_3$ between PA6/PP/5M/25C-1 and PA6/PP/5M/25C-2 can be understood concerning the interaction among different components and the migration of $CaCO_3$ during compounding. For directly mixed PA6/PP/5M/25C-1, the melting of PP and MAPP happened before that of PA6 and $CaCO_3$ entered PP and MAPP melt first. During this time, some $CaCO_3$ particles had opportunity to interact with MAPP and became encapsulated by MAPP molecules. After the melting of PA6, a certain amount of $CaCO_3$ migrated to PA6 phase, but the $CaCO_3$ encapsulated by MAPP wouldn't and finally ended up in PP phase. While for PA6/PP/5M/25C-2, $CaCO_3$ was premixed with PA6, thus the reaction of PA6 with MAPP competed with the interaction between $CaCO_3$ with MAPP when all components melted in the second step. Because of the high reactivity between MAPP and PA6, fewer $CaCO_3$ particles got encapsulated by MAPP. This might be the reason why the amount of $CaCO_3$ in PP phase for PA6/PP/5M/25C-1 is higher than that for PA6/PP/5M/25C-2.

To verify the above mentioned hypothesis, $CaCO_3$-filled PA6/PP blend was prepared by direct mixing in the absence of MAPP. The sample is designated as PA6/PP/25C. The amount of $CaCO_3$ in PP phase for PA6/PP/25C is 44.6% (see Table II),

Table II. Distribution Ratio of $CaCO_3$ in PP and PA6 Phases for All Filled PA6/PP Blends

	$CaCO_3$ in PP phase	$CaCO_3$ in PA6 phase
PA6/PP/5M/25C-1	74.6%	25.4%
PA6/PP/5M/25C-2	53.3%	46.7%
PA6/PP/25C	44.6%	55.4%

which is lower than that for PA6/PP/5M/25C-1 and PA6/PP/5M/25C-2, thus our hypothesis is correct. Ersoy et al.[23] found that most of the incorporated $CaCO_3$ was located in PA6 phase for $CaCO_3$-filled PA6/PP blend without compatibilizer. This is clearly different from our result (44.6% of $CaCO_3$ in PP phase). On one hand, this could be ascribed to a difference in the surface characteristics of $CaCO_3$ used in the two cases. On the other hand, the tendency of fillers to be located in the more viscous phase (PP is more viscous than PA6 phase in our case) to minimize energy dissipation during compounding might also play a role.[28]

Mechanism of Morphology Formation

A possible mechanism is brought up based on the distribution states of $CaCO_3$ and the characteristics of injection flow. First, polymer melt experiences intense shear and elongational stresses along the flow direction during the entire filling stage, which can cause dispersed phase to be stretched in the same direction. The coalescence of dispersed domains is another factor that can not be neglected. D'Orazio et al. have reported irregularly shaped EPR domains in the core of injection-molded iPP/EPR (80/20 w/w) blend due to the coalescence phenomenon.[24] In our case, the volume fraction of PP phase reaches 35, 39, and 37% for PA6/PP/5M, PA6/PP/5M/25C-1, and PA6/PP/5M/25C-2, respectively, making the coalescence of dispersed droplets unavoidable. Thus during the filling stage high shear and elongational flow fields facilitate dispersed PP droplets to be stretched along the flow direction and coalesce into strips in the core.

Second, coalescence, relaxation and breakup of dispersed phase compete with solidification process of polymer melt after the cessation of injection flow. In the present case, it is reasonable that it takes only a few seconds to cool down the polymer melt below the melting temperature of PA6. For unfilled sample PA6/PP/5M, PP domains in the core have enough time to coalesce completely and relax or break up into spherical or ellipsoidal shape when the mould-filling stage is finished. However, the situation is quite different for $CaCO_3$-filled samples. The incorporation of $CaCO_3$ greatly altered the rheological properties of the two phases, causing the characteristic times of particle coalesce, shape relaxation, and breakup to exceed the solidification time of polymer melt greatly. Thus, in the presence of $CaCO_3$, it is difficult for PP domains to coalesce completely, and it is also difficult for PP strips in the core to relax or break up into spherical domains. Fenouillot et al.[29] have reported that for a blending system in which dispersed phase could crosslink, coagulation instead of coalescence happens when the gel fraction of dispersed phase reached a certain value. PP phase filled by a large amount of $CaCO_3$ can behave in a similar way to crosslinked dispersed phase. Incomplete coalescence or so called coagulation of PP domains leads to the formation of nodes on PP strips. Compared to PA6/PP/5M/25C-2, more $CaCO_3$ is distributed in PP phase (74.6%) of PA6/PP/5M/25C-1, therefore the deformation and complete coalescence of PP phase proceed more slowly. This is why the density of nodes on PP phase of PA6/PP/5M/25C-1 is larger than that of PA6/PP/5M/25C-2. On the other hand, deformed PP phase does not have enough time to relax or break up before the morphology is frozen at last due to the incorporation of $CaCO_3$. This explains why different types of morphology are formed in the core region for unfilled and $CaCO_3$-filled PA6/PP/MAPP blends.

Third, the difference in the size of PP phase in the core region for $CaCO_3$-filled samples originates from different compatibilization efficiency of MAPP. The compatibilization efficiency of MAPP in PA6/PP/5M/25C-2 which is prepared by masterbatch approach is higher than that in one-step compounded PA6/PP/5M/25C-1. This is because more MAPP molecules encapsulate $CaCO_3$ particles and less MAPP can locate at interface acting as compatibilizer for PA6/PP/5M/25C-1. Therefore, initial size of PP domains before injection molding in PA6/PP/5M/25C-2 is smaller than that in PA6/PP/5M/25C-1. The effects of *in situ* compatibilizer on the morphology development of polymer blends are rather complicated. On one hand, it can facilitate the deformation and breakup of droplets by reducing interfacial tension or enhancing interfacial adhesion. On the other hand, it can also stabilize droplets by reducing coalescence or increasing interfacial viscosity.[21] Considering that the rheological properties of the two phases are greatly altered by adding $CaCO_3$, the former case mentioned above may be dominating. Thus, the high compatibilization efficiency of MAPP for PA6/PP/5M/25C-2 ensures effective stress transfer from PA6 to PP phase and considerable deformation of PP domains. As a result, finer and looser network structure of PP phase is formed in PA6/PP/5M/25C-2.

Last, PP domains in the subskin exist as platelets, meaning that they are also deformed perpendicular to the flow direction. This is the result of spreading radial flow at the entrance of the mould.[25] The spreading flow can cause shear and elongational fields perpendicular to the flow direction, leading to the deformation of PP domains in the traverse direction. The effect of spreading flow is confined in a limited zone (near the gate) and is milder compared to the flow fields parallel to the flow direction. Thus, PP platelets in the subskin are longer in the direction parallel to injection flow.

Mechanical Properties and HDT

Table III gives the mechanical properties and HDT of PA6/PP/5M, PA6/PP/5M/25C-1, and PA6/PP/5M/25C-2. The addition of $CaCO_3$ brings about remarkable increase in the impact strength of PA6/PP/MAPP blend and PA6/PP/5M/25C-1 outperforms over PA6/PP/5M/25C-2, with its dry state impact strength 53.3% higher than the unfilled sample PA6/PP/5M. There may be two reasons for the high impact strength of PA6/PP/5M/25C-1: (1) more $CaCO_3$ was distributed in PP phase for PA6/PP/5M/25C-1, which leads to a higher volume fraction of PP phase and thus higher toughening efficiency of PP phase; (2) the ginger-like morphology in the core region may contribute to improved toughness by retarding the development of microcracks[30] or absorbing more energy through debonding and friction[31] between PA6 and PP phases during impact test.

The addition of $CaCO_3$ causes the flexural strength and tensile strength to decrease more or less and the worsening is smaller for PA6/PP/5M/25C-2. Considering the morphological differences, this is not difficult to understand. The morphology of PA6/PP/5M/25C-2 is finer than that of PA6/PP/5M/25C-1 and its

Table III. Mechanical Properties and HDT

	Tensile strength (MPa)	Tensile modulus (MPa)	Flexural strength (MPa)	Flexural modulus (MPa)	Impact strength (J m^{-1})	HDT (°C)
PA6/PP/5M	61.7 ± 0.2 (52.9 ± 0.4)[a]	860 ± 34 (814 ± 12)	100.8 ± 1.2 (82.2 ± 0.8)	2187 ± 37 (1686 ± 14)	16.1 (19.9)	93.0
PA6/PP/5M/25C-1	51.9 ± 0.1 (45.1 ± 0.1)	(1119 ± 8) 1035 ± 8	80.4 ± 1.2 (62.0 ± 0.9)	2303 ± 34 (1597 ± 24)	27.4 (30.5)	108.1
PA6/PP/5M/25C-2	53.0 ± 2.8 (48.1 ± 3.7)	859 ± 39 (840 ± 19)	94.1 ± 0.2 (80.8 ± 2.3)	2304 ± 40 (1985 ± 78)	20.7 (23.6)	125.0

[a]Wet state data are placed in parenthesis and the others are dry state data.

interfacial adhesion between PA6 and PP phases is better. As a result, tensile load can be transferred from PA6 phase to PP phase more effectively. Moreover, PA6/PP/5M/25C-2 has a larger amount of $CaCO_3$ in PA6 matrix, which is also beneficial to the strength of the blend. The addition of $CaCO_3$ brings about different effects on the tensile and flexural modulus of samples prepared by different compounding sequences. The tensile modulus of PA6/PP/5M/25C-1 is larger than that of PA6/PP/5M/25C-2, while its wet state flexural modulus is smaller than that of PA6/PP/5M/25C-2. It is difficult to give a reliable explanation to this result and we speculate that different structural features ($CaCO_3$ distribution, interfacial tension, etc.) have different extent of contributions to the tensile and flexural modulus of the composites.

The HDT of PA6/PP/5M/25C-2 is 32.0°C higher than that of PA6/PP/5M, while the HDT of PA6/PP/5M/25C-1 is only 14.0°C over that of PA6/PP/5M. This is determined by the difference in the distribution state of $CaCO_3$ in the blend. More $CaCO_3$ was distributed in PA6 matrix for PA6/PP/5M/25C-2, so the increment in HDT for PA6/PP/5M/25C-2 is larger.

CONCLUSIONS

The effects of $CaCO_3$ and different compounding sequences on the phase morphology of MAPP compatibilized PA6/PP blend have been investigated. In the core region of injection molded specimen, the addition of $CaCO_3$ led to oriented ginger-like network of PP phase for the one-step compounded sample and finer and looser elongated network for the sample prepared by masterbatch approach. Deformation, incomplete coalescence and retarded relaxation (or breakup) of PP phase in the presence of $CaCO_3$ are believed to be the mechanism for morphology formation. The morphological differences between the samples prepared by the two compounding sequences originate from the different distribution of $CaCO_3$ in the two phases and compatibilization efficiency of MAPP. Because of the different morphology formed, the $CaCO_3$-filled PA6/PP/MAPP blends exhibit superior properties in different aspects. The impact strength of the one-step compounded $CaCO_3$-filled sample is 53.3% higher than that of unfilled sample. The HDT of $CaCO_3$-filled sample prepared by masterbatch approach is 32.0°C higher than that of unfilled sample.

REFERENCES

1. Utracki, L. A. Commercial Polymer Blends; Chapman & Hall: London, **1998.**
2. Bucknall, C. B. Toughened Plastics; Applied Science Publishers: London, **1977.**
3. Wang, Y.; Zhang, Q.; Fu, Q. *Macromol. Rapid Commun.* **2003,** *24*, 231.
4. Khatua, B. B.; Lee, J. D.; Kim, H. Y.; Kim, J. K. *Macromolecules* **2004,** *37*, 2454.
5. Ray, S. S.; Bousmina, M. *Macromol. Rapid Commun.* **2005,** *26*, 450.
6. Li, Y. J.; Shimizu, H. *Polymer* **2004,** *45*, 7381.
7. Li, Y. J.; Shimizu, H. *Macromol. Rapid Commun.* **2005,** *26*, 710.
8. Filippone, G.; Dintcheva, N. T.; Acierno, D.; La Mantia, F. P. *Polymer* **2008,** *49*, 1312–1322.
9. Ersoy, O. G.; Nugay, N. *Polymer* **2004,** *45*, 1243.
10. Olmos, D.; González-Benito, J. *Eur. Polym. J.* **2007,** *43*, 1487.
11. Chen, P.; Chen, J.; He J. S. *J. Polym. Sci. B: Polym. Phys.* **2009,** *47*, 25.
12. Sahnoune, F.; Lopez Cuesta, J. M.; Crespy, A. *Polym. Eng. Sci.* **2003,** *43*, 647.
13. Xie, T. X.; Liu, H. Z.; Ou, Y. C.; Yang, G. S. *J. Appl. Polym. Sci.* **2006,** *101*, 3361.
14. Yang, Y. L.; G'Sell, C.; Hiver, J. M.; Bai, S. L. *J. Appl. Polym. Sci.* **2007,** *103*, 3907.
15. Xie, T. X.; Liu H. Z.; Ou Y. C.; Yang, G. S. *J. Polym. Sci. Part B: Polym. Phys.* **2005,** *43*, 3213.
16. Yang, Y. L.; Bai, S. L.; G'Sell, C.; Hiver, J. M. *Polym. Eng. Sci.* **2006,** *46*, 1512.
17. Premphet, K.; Horanont, P. *Polym. Plast. Technol. Eng.* **2001,** *40*, 235.
18. Zhang, L.; Wang, Z. H.; Huang, R.; Li, L. B.; Zhang, X. Y. *J. Mater. Sci.* **2002,** *37*, 2615.
19. Premphet-Sirisinha, K.; Preechachon, I. *J. Appl. Polym. Sci.* **2003,** *89*, 3557.
20. Zheng, M. J.; Li, H. L. *J. Appl. Polym. Sci.* **2004,** *91*, 1635.
21. Pötschke, P.; Paul, D. R. *J. Macromol. Sci. Polym. Rev.* **2003,** *C43*, 87.

22. Holsti-Miettinen, R. M.; Perttila, K. P.; Seppälä, J. V.; Heino, M. T. *J. Appl. Polym. Sci.* **1995,** *58*, 1551.
23. Ersoy, O. G.; Nugay, N. *Compos. A* **2007,** *38*, 162.
24. D'Orazio, L.; Mancarella, C.; Martuscelli, E.; Cecchin, G.; Corrieri, R. *Polymer* **1999,** *40*, 2745.
25. Walling, N.; Kamal, M. R. *Adv. Polym. Technol.* **1996,** *5*, 269.
26. Fisher, I.; Siegmann, A.; Narkis, M. *Polym. Compos.* **2002,** *23*, 34.
27. Zhong, G. J.; Li, Z. M. *Polym. Eng. Sci.* **2005,** *45*, 1655.
28. Persson, A. L.; Bertilsson, H. *Polymer* **1998,** *39*, 5633.
29. Fenouillot, F.; Perier-Camby, H. *Polym. Eng. Sci.* **2004,** *44*, 625.
30. Özden, E.; Menceloglu, Y. Z.; Papila, M. *ACS Appl. Mater. Inter.* **2010,** *2*, 1788.
31. Ichinose, N.; Ishikawa, M.; Morimoto, K. *Polym. Compos.* **2011,** *32*, 1617.